JBC RESEARCH ARTICLE

Mutagenesis of bracelet cyclotide hyen D reveals functionally and structurally critical residues for membrane binding and cytotoxicity

Received for publication, September 14, 2021, and in revised form, February 19, 2022 Published, Papers in Press, March 11, 2022,
https://doi.org/10.1016/j.jbc.2022.101822

Qingdan Du (杜清丹),[‡], Yen-Hua Huang (黃彥華),[*,‡], Conan K. Wang, Quentin Kaas, and David J. Craik[*]

From the Institute for Molecular Bioscience, Australian Research Council Centre of Excellence for Innovations in Peptide and Protein Science, The University of Queensland, Brisbane, QLD, Australia

Edited by Wolfgang Peti

Cyclotides have a wide range of bioactivities relevant for agricultural and pharmaceutical applications. This large family of naturally occurring macrocyclic peptides is divided into three subfamilies, with the bracelet subfamily being the largest and comprising the most potent cyclotides reported to date. However, attempts to harness the natural bioactivities of bracelet cyclotides and engineer-optimized analogs have been hindered by a lack of understanding of the structural and functional role of their constituent residues, which has been challenging because bracelet cyclotides are difficult to produce synthetically. We recently established a facile strategy to make the I11L mutant of cyclotide hyen D that is as active as the parent peptide, enabling the subsequent production of a series of variants. In the current study, we report an alanine mutagenesis structure-activity study of [I11L] hyen D to probe the role of individual residues on peptide folding using analytical chromatography, on molecular function using surface plasmon resonance, and on therapeutic potential using cytotoxicity assays. We found that Glu-6 and Thr-15 are critical for maintaining the structure of bracelet cyclotides and that hydrophobic residues in loops 2 and 3 are essential for membrane binding and cytotoxic activity, findings that are distinct from the structural and functional characteristics determined for other cyclotide subfamilies. In conclusion, this is the first report of a mutagenesis scan conducted on a bracelet cyclotide, offering insights into their function and supporting future efforts to engineer bracelet cyclotides for biotechnological applications.

Cyclotides are the largest family of ribosomally synthesized cyclic peptides from plants (1–3). They are characterized by a head-to-tail cyclic backbone and three interlocked disulfide bonds. Due to their unique three-dimensional structure, they are exceptionally stable, making them attractive leads in high-value biotechnological applications. Their natural function is in defense against insects and pathogens (4), and this activity recently led to their use in agriculture, with Sero-X being the first cyclotide-containing plant extract bio-pesticide (https://innovate-ag.com.au/). Aside from their natural function, native cyclotides have numerous other bioactivities, many of which are medically relevant, including anthelmintic (5), anti-HIV (6), cytotoxic (7), immunosuppressive (8), and aphrodisiac activities (9), suggesting that they have a range of potential therapeutic applications.

Cyclotides are classified into three subfamilies – the bracelet, Möbius, and trypsin inhibitor subfamilies. The bracelet and Möbius subfamilies are similar in both amino acid sequence and function and differ from the trypsin inhibitor subfamily, although all subfamilies share a cystine knot core and a cyclic backbone (10). The six inter-cysteine sequence segments in cyclotides are referred to as "loops". Möbius cyclotides are distinguished from bracelet cyclotides by the presence of a *cis*-Pro residue in loop 5 as well as different sets of sequences in loops (3, 11). Prototypical cyclotides for the Möbius and bracelet subfamilies are kalata B1 (kB1, Fig. 1*A*) (12) and cycloviolacin O2 (cyO2, Fig. 1*B*) (13), respectively. An analysis of the sequences of the two subfamilies identifies distinct patterns. As shown in Figure 1*C* the exemplary sequence alignment for loop 2 of bracelet cyclotides displays the pattern "VXIP", with *X* representing the aromatic residues Trp, Tyr, or Phe, whereas loop 2 sequences of Möbius cyclotides are more hydrophilic. Bracelet cyclotides have a longer loop 3 sequence, of six to seven residues forming a helical structure, whereas Möbius cyclotides typically only have four residues in that loop. Finally, bracelet cyclotides have more cationic residues in loop 5 than Möbius cyclotides. The various sequence and structural differences between these two subfamilies prompted us to investigate the potential roles of these residues in cyclotide bioactivities.

According to CyBase (http://www.cybase.org.au/), a database of ribosomally synthesized, backbone-cyclic peptides (14, 15), the bracelet subfamily makes up two thirds of the whole cyclotide family, making them the largest pool of candidates for future applications. Their abundance suggests they might have advantageous properties over Möbius cyclotides. Amongst many bioactivity studies of cyclotides, the most active molecules typically belong to the bracelet subfamily. For example, in one study cyO2 and two Möbius cyclotides, varv A and varv F, were examined for their cytotoxicity against 10

[‡] These authors contributed equally to this work.
[*] For correspondence: David J. Craik, d.craik@imb.uq.edu.au; Yen-Hua Huang, y.huang@imb.uq.edu.au.

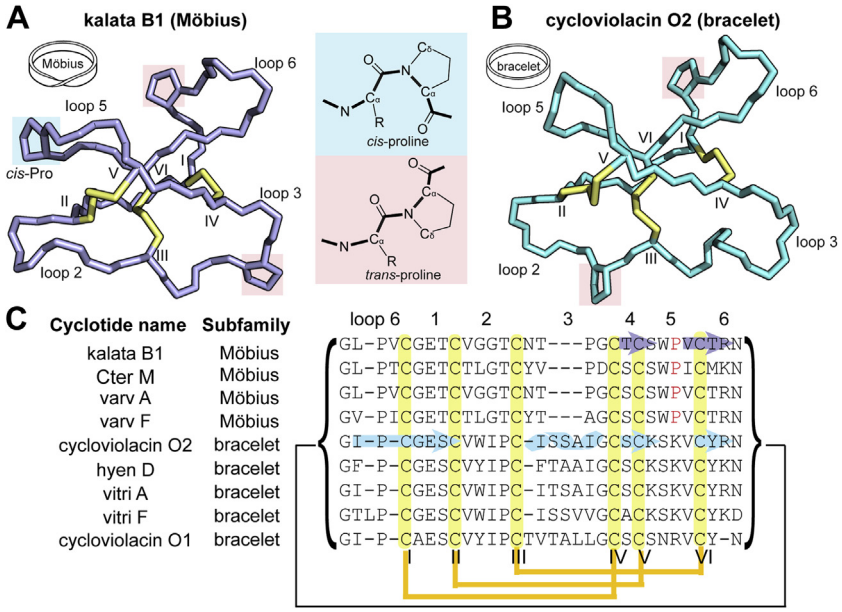

Figure 1. Three-dimensional structures of prototypical cyclotides of the two major subfamilies and an illustration of *cis*- and *trans*-proline conformations. Three-dimensional structures of the prototypical cyclotides from Möbius (*A*) and bracelet (*B*) cyclotide subfamilies. The NMR solution structures of kalata B1 and cycloviolacin O2 are from PDB files 1NB1 and 2KNM, respectively (12, 13). *C*, alignment of exemplary cyclotides from bracelet and Möbius subfamilies. The *orange* and *black* lines, respectively, represent the disulfide bonds and the cyclic backbone. Cysteine residues are highlighted in *yellow*. The Pro residue in loop 5 of Möbius cyclotides that adopts a *cis* conformation is in *red*. The structural features of the prototypical cyclotides kB1 and cyO2 are highlighted in *purple* or *blue*. Each β-strand is depicted by an *arrow*, and the 3_{10} helix is depicted by a short helix (*blue*).

human tumor cell lines, and it was found that cyO2 was over 20-fold more potent compared to varv A and varv F (16). In another study, three bracelet cyclotides, cyO2, vitri A, and vitri F, were over ten-fold more active than 11 Möbius cyclotides against five cancer cell lines (17).

As reported previously, cyclotides from both bracelet and Möbius subfamilies deliver their bioactivities, including cytotoxic, hemolytic, anthelmintic, nematocidal, insecticidal, and antiretroviral activities through membrane binding (7, 18–20). However, our current understanding of the molecular mechanism of action of cyclotides has been largely based on structure-activity relationship (SAR) studies of Möbius cyclotides. Alanine and lysine scanning mutagenesis studies of the Möbius cyclotide kB1 combined with kB1-membrane interaction studies have clearly mapped out the residues involved in its function (18, 21, 22). These studies demonstrate that Gly-6, Glu-7, Thr-8, Asn-15, and Thr-16 of kB1 form a 'bioactive face' that is crucial for insecticidal activity, and hydrophobic residues in loops 2, 5, and 6 form a 'hydrophobic face' that is responsible for driving insertion into the membrane (23). However, whether these findings can be applied to the function of bracelet cyclotides has been difficult to answer without a systematic mutagenesis study of bracelet cyclotides. Until now, efforts to explore their SAR have been hampered by the synthetic intractability of bracelet cyclotides.

Hyen D (amino acid sequence shown in Fig. 1*C*) is the most abundant and active cyclotide present in the medicinal herb *Hybanthus enneaspermus* and belongs to the bracelet subfamily (7). Hyen D is one of the most cytotoxic cyclotides reported and therefore has great potential in anti-cancer applications. Although hyen D has a poor folding yield using the conventional oxidative folding conditions that are successful for kB1, we recently reported that a single conservative amino acid substitution, Ile-11 to Leu, could markedly improve its folding yield (24). Importantly, the mutant I11L retains the cytotoxicity and membrane-binding properties of wild-type (WT) hyen D. In the current study, we found that [I11L] hyen D (referred to hereafter as I11L) adopts the same three-dimensional structure as its parent peptide using NMR spectroscopy. Taking advantage of this folding-accessible mutant, we synthesized a series of alanine mutants of I11L. Effects of the substitutions on folding, membrane binding, and cytotoxicity were evaluated. This study is the first alanine-scan mutagenesis study reported on a member from the bracelet subfamily, shedding light on the key residues for the folding and activity of bracelet cyclotides.

Results

NMR solution structure of hyen D

Hyen D has six residues that are different from the prototypical bracelet cyclotide cyO2 but exhibits comparable activity (7). As hyen D forms the basis of this study, native hyen D was extracted from *H. enneaspermus* and its solution structure was determined using NMR spectroscopy. Peaks in the ^{1}H one-dimensional spectrum were sharp and well-dispersed across the amide region (Fig. S1), indicating that hyen D adopts a rigid and well-defined structure. Subsequently, a series of two-dimensional NMR experiments were recorded and analyzed: TOCSY, NOESY, ^{15}N heteronuclear single quantum coherence (HSQC), ^{13}C HSQC, and exclusive COSY (E-COSY). A total of 365 distance restraints were

determined from the NOESY spectra, and 24 dihedral angle restraints were derived using coupling constants from one-dimensional and E-COSY spectra. Eight hydrogen bonds were suggested from the deuterium exchange of amide protons and amide temperature coefficients. The distance and other structural restraints as well as structural statistics are summarized in Table 1.

Using distance, dihedral, hydrogen-bond restraints, and disulfide-bond restraints, 50 structures were calculated by means of torsion angle simulated annealing. A superimposition of the 20 lowest-energy structures obtained after energy minimization is shown in Figure 2*A*. Most regions of the structure are well defined, with an average RMSD of 0.48 Å for the backbone atoms and 1.11 Å for all heavy atoms.

Based on the analyses of preliminary structures using MOLMOL, the hydrogen bond donors were assigned to be Phe-2, Cys-4, Cys-8, Ala-16, Val-26, Cys-27, Tyr-28, and Lys-29, and their corresponding bond acceptors were Lys-29, Cys-27, Lys-25, Cys-13, Lys-23, Glu-6, Ser-21, and Phe-2, respectively. The secondary structure characteristics and hydrogen bond network of hyen D are shown in Figure 2*B*.

The solution structure of hyen D has a small 3_{10} helix in loop 3, comprising residues Cys-13 to Gly-19. This loop 3 helix is typically present in bracelet cyclotides but is not in Möbius cyclotides (12, 13). Hyen D also has a β-sheet that comprises three strands and two β-turns and incorporates residues in loops 1, 4, 5, and 6. As described above, the structure of hyen D is stabilized by a series of hydrogen bonds including one formed by the side chain of Glu-6 (loop 1), interacting with Phe-14 and Thr-15 in loop 3. In addition to these hydrogen bonds, three disulfide bonds that form a cystine knot reinforce the structure. Overall, the tertiary structure of hyen D is similar to those of other bracelet cyclotides characterized by NMR, including cycloviolacin O1 (3, 25), cyO2 (13), and kalata B5 (26) as shown in Figure 2*C*, confirming that bracelet cyclotides share a conserved topology.

Synthesis and folding of I11L and its alanine variants

The increase in synthesis yield on substitution of Ile-11 for Leu in bracelet cyclotides is very significant (24). For instance, [I11L]hyen D (I11L) achieved 44% correctly folded product within 12 h using a slightly modified folding condition from that reported for kB1 (27), whereas the yield of correctly folded hyen D was negligible under the same conditions.

The NMR solution structure of I11L was compared to that of WT hyen D by analyzing their secondary Hα NMR chemical shifts determined from TOCSY and NOESY spectra and Hα random coil chemical shifts (28). Secondary Hα chemical shifts provide information on secondary structure content (29). As seen from Figure 2*D*, I11L displays secondary Hα shifts almost identical to the native peptide, confirming that it adopts the same conformation as WT hyen D. Since I11L is reported to retain the same membrane-binding ability as hyen D (24), it is proposed that the I11L mutant could be used as a surrogate for the native peptide in biotechnological applications. To further understand the SAR of I11L, we carried out an alanine mutagenesis study.

Each residue of I11L was successively mutated to alanine to investigate their role in mediating function, except for the two Ala residues in loop 3 and six Cys residues. The amino acid sequences of the Ala mutants and their *in vitro* folding yields are summarized in Table 2, with the HPLC folding traces shown in Fig. S2. All Ala variants could be produced synthetically except [P3A], [E6A], [P12A], [G19A], and [T15A] I11L. [E6A], [T15A], and [G19A]I11L did not achieve native folding, while the two proline variants could not be assembled in sufficient yield for further studies. All peptides synthesized and folded were purified to >95% purity as evaluated by analytical HPLC and LC/MS; purity traces and MS spectra are shown in Fig. S3.

The secondary structures of the I11L alanine variants were compared to those of I11L and hyen D by analyzing their secondary Hα chemical shifts (Fig. 3). All alanine mutants that could be folded had chemical shifts similar to those of both I11L and WT hyen D, with only minor local shift perturbations at the substituted residues, suggesting that they all adopt the native conformation of hyen D (1D proton NMR spectra are shown in Fig. S1).

Lipid binding of hyen D, I11L, and I11L variants

To investigate the function of the alanine mutants, we evaluated their binding affinity for the model lipid membrane using surface plasmon resonance (SPR). The Möbius cyclotide kB1 was included in these experiments as a reference. Binding to phosphatidylethanolamine-containing membranes is central

Table 1
Geometric and energetic statistics for the 20 lowest-energy solution structures of hyen D

NMR constraints		Structure statistics (Violations, mean ± SD)	
Distance constraints		Distance constraints (Å)	0 ± 0
Total NOE	365	Dihedral angle constraints (°)	1.404
Intra residue	95	Maximum distance constraint violation (Å)	0
Inter residue	270	Maximum dihedral angle violation (°)	0.59 ± 0.46
Sequential ($\|i-j\| = 1$)	139	Deviations from idealized geometry	
Medium-range ($\|i-j\| \leq 4$)	55	Bond lengths (Å)	0.015 ± 0.0009
Long-range ($\|i-j\| \geq 5$)	96	Bond angles (°)	1.50 ± 0.0420
Hydrogen bonds	8	Impropers (°)	1.49 ± 0.1140
Dihedral angle constraints		Average pairwise RMSD (Å) for 20 refined structures	
Total dihedral angles	24	Backbone	0.48 ± 0.14
Φ	15	Heavy	1.11 ± 0.21
χ^1	9	Ramachandran statistics	
		Most favored (%)	89.5

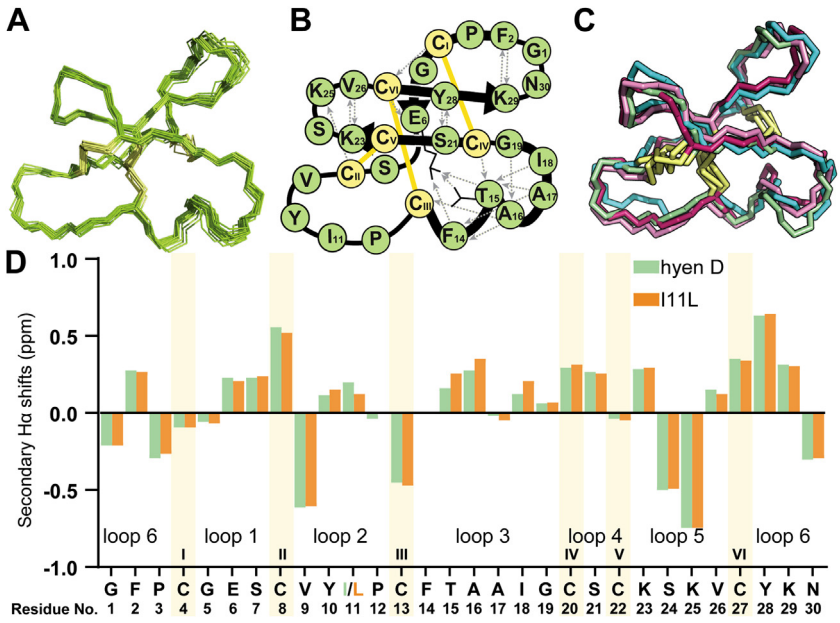

Figure 2. Structural characterization of hyen D and I11L using NMR. *A*, superimposition of the 20 lowest-energy models of the hyen D solution structure computed from NMR data. *B*, schematic view of the secondary structure of hyen D. Hydrogen bonds are shown as *gray-dashed arrows*, β-strands are shown as *black arrows*, and the 3_{10} helix is shown as a *black ribbon*. *C*, structure comparison between cycloviolacin O1 (*hot pink*), cyO2 (*cyan*), kalata B5 (*pink*), and hyen D (*green*). *D*, secondary Hα chemical shifts of I11L (*orange*) compared to hyen D (*green*). Residue number, loop position, and Roman numeral for each cysteine are provided above the sequence. Secondary Hα chemical shifts provide information on secondary structure as indicated by Wishart *et al* (29). A group of four or more consecutive residues with secondary Hα chemical shifts less than −0.1 is likely to adopt a helical structure, whereas a cluster of three or more residues with values more than 0.1 is likely to be a β-strand.

to the function of Möbius and bracelet cyclotides because it causes membrane perturbations that ultimately lead to membrane disruption (30–32). Therefore, the SPR lipid-binding experiments were carried out with a model membrane composed of 20% 1-palmitoyloleoyl-phosphatidylethanolamine (POPE) and 80% 1-palmitoyloleoyl-phosphatidylcholine (POPC). The membrane-binding affinity of cyclotides was evaluated by measuring the cyclotide/lipid maximum binding ratio (P/L max, mol/mol) and the cyclotide concentration that is required to reach half-maximum binding of I11L (K_D).

As shown in Table 3 and Fig. S4, the Ala mutations had varying effects on activity relative to the parent peptide I11L, with substitutions in loops 2 and 3 having the most impact. For example, the loop 2 mutant [Y10A]I11L displayed a 2.5-fold decrease in P/L max compared to I11L, whereas other alanine mutants displayed smaller changes in that

Table 2
Sequence alignment, mass, and folding yield[a] of I11L and its alanine variants

Peptide name	Mutating loop	Amino acid sequence	Average mass (Da)	Folding yield[b]
hyen D	–	GFPCGESCVYIPCFTAAIGCSCKSKVCYKN	3155.7	<1
I11L	2	GFPCGESCVY**L**PCFTAAIGCSCKSKVCYKN	3155.7	100
[G1A]I11L	6	**A**FPCGESCVYLPCFTAAIGCSCKSKVCYKN	3169.7	13
[F2A]I11L	6	G**A**PCGESCVYLPCFTAAIGCSCKSKVCYKN	3079.7	43
[P3A]I11L	6	GF**A**CGESCVYLPCFTAAIGCSCKSKVCYKN	3129.7	–
[G5A]I11L	1	GFPC**A**ESCVYLPCFTAAIGCSCKSKVCYKN	3169.7	14
[E6A]I11L	1	GFPCG**A**SCVYLPCFTAAIGCSCKSKVCYKN	3097.7	<1
[S7A]I11L	1	GFPCGE**A**CVYLPCFTAAIGCSCKSKVCYKN	3139.7	18
[V9A]I11L	2	GFPCGESC**A**YLPCFTAAIGCSCKSKVCYKN	3127.7	39
[Y10A]I11L	2	GFPCGESCV**A**LPCFTAAIGCSCKSKVCYKN	3063.7	26
[L11A]I11L	2	GFPCGESCVY**A**PCFTAAIGCSCKSKVCYKN	3113.7	44
[P12A]I11L	2	GFPCGESCVYL**A**CFTAAIGCSCKSKVCYKN	3129.7	–
[F14A]I11L	3	GFPCGESCVYLPC**A**TAAIGCSCKSKVCYKN	3079.7	60
[T15A]I11L	3	GFPCGESCVYLPCF**A**AAIGCSCKSKVCYKN	3125.7	<1
[I18A]I11L	3	GFPCGESCVYLPCFTAA**A**GCSCKSKVCYKN	3113.7	26
[G19A]I11L	3	GFPCGESCVYLPCFTAAI**A**CSCKSKVCYKN	3169.7	<1
[S21A]I11L	4	GFPCGESCVYLPCFTAAIGC**A**CKSKVCYKN	3139.7	11
[K23A]I11L	5	GFPCGESCVYLPCFTAAIGCSC**A**SKVCYKN	3098.7	12
[S24A]I11L	5	GFPCGESCVYLPCFTAAIGCSCK**A**KVCYKN	3139.7	50
[K25A]I11L	5	GFPCGESCVYLPCFTAAIGCSCKS**A**VCYKN	3098.7	13
[V26A]I11L	5	GFPCGESCVYLPCFTAAIGCSCKSK**A**CYKN	3127.7	68
[Y28A]I11L	6	GFPCGESCVYLPCFTAAIGCSCKSKVC**A**KN	3063.7	49
[K29A]I11L	6	GFPCGESCVYLPCFTAAIGCSCKSKVCY**A**N	3098.7	19
[N30A]I11L	6	GFPCGESCVYLPCFTAAIGCSCKSKVCYK**A**	3112.7	17

[a] Alanine variants of I11L and hyen D were folded under 50% isopropanol in 0.1 M ammonium bicarbonate (pH 8.5), supplemented with GSH/GSSG (2:0.8 mM) for 12 h. I11L was folded under similar folding condition except with 45.5% isopropanol.
[b] The folding yield is relative to I11L at 100%.

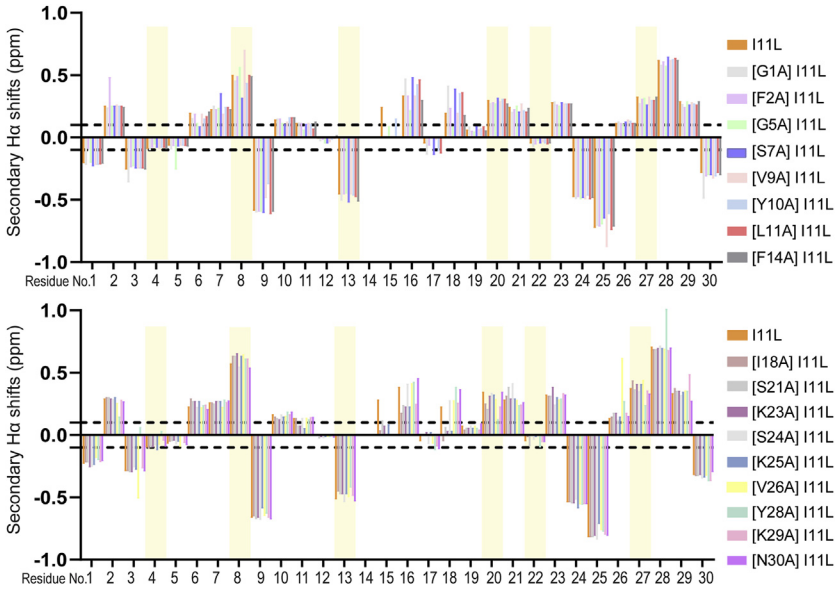

Figure 3. Hα secondary NMR chemical shifts of I11L and its Ala mutants compared to I11L and native hyen D. The Hα chemical shifts for Phe-14 and Thr-15 are missing in the spectra for most peptides. Cysteine residues are highlighted in *yellow*.

measurement. With respect to K_D values, mutations carried out in loop 2 also had the largest effect, with increased K_D values by four-to ten-fold compared to I11L. Mutations carried out in loop 3 also had significant impact on K_D, which was increased by three-fold compared to I11L. In loop 5, the K_D value of [V26A]I11L increased by 2-fold compared to that of I11L, but substitution with Ala for the other three positions led to no change in activity. Substitutions in loops 1 and 6 caused a two-fold or less change in K_D. The lipid-binding affinity was weakened for one of the loop 1 mutants, [S7A]I11L, whereas the other loop 1 mutant [G5A]I11L displayed comparable activity to I11L. Overall, the ranking in terms of importance for membrane-binding of the six loops of I11L is loop 2 > loop 3 > loop 1 ≥ loop 5 > loop 6 ≥ loop 4.

Cytotoxicity evaluation of hyen D, I11-L and its variants

To examine the effect of single residue substitutions on biological activity, cytotoxicity against HeLa cells was evaluated. Mammalian cancer cells can be used as a predictor of cyclotide activity because the extracellular leaflet of the plasma membrane displays PE lipids (33). Cytotoxicity was evaluated according to the cyclotide concentration required to kill half of the cells (CC_{50}, μM), values for which are shown in Table 3 and Fig. S4. Most of the Ala variants had a decrease in cytotoxicity against cancer cells compared to I11L, albeit to different extents, with some retaining or slightly enhancing the activity of I11L and none completely lacking cytotoxic activity.

Consistent with their binding affinities for model membranes, the largest changes in cytotoxic activity were for loop 2

Table 3
Cytotoxicity[a] and membrane binding affinity of the hyen D variants

Peptide	Mutated loop	POPC/POPE (80:20)		CC_{50} on HeLa (μM)	Fold of activity loss[b]
		P/L max (mol/mol)	K_D (μM)		
hyen D	–	0.31 ± 0.00	5.88 ± 0.07	0.92 ± 0.07	–
I11L	2	0.30 ± 0.00	5.80 ± 0.03	1.08 ± 0.04	1.00
[G1A] I11L	6	0.30 ± 0.01	5.54 ± 0.19	0.69 ± 0.02	0.64
[F2A] I11L	6	0.23 ± 0.01	13.1 ± 0.88	2.85 ± 0.10	2.64
[G5A] I11L	1	0.29 ± 0.00	4.77 ± 0.16	1.29 ± 0.06	1.19
[S7A] I11L	1	0.27 ± 0.01	8.73 ± 0.50	4.15 ± 2.88	3.84
[V9A] I11L	2	0.28 ± 0.01	29.5 ± 1.29	6.01 ± 1.21	5.56
[Y10A] I11L	2	0.12 ± 0.01	55.7 ± 0.10	4.27 ± 0.34	3.95
[L11A] I11L	2	0.26 ± 0.02	21.5 ± 0.45	8.64 ± 1.21	8.00
[F14A] I11L	3	0.28 ± 0.02	19.4 ± 0.80	4.10 ± 0.39	3.80
[I18A] I11L	3	0.19 ± 0.01	14.7 ± 1.80	3.99 ± 0.21	3.69
[S21A] I11L	4	0.32 ± 0.01	4.20 ± 0.23	1.26 ± 0.08	1.17
[K23A] I11L	5	0.28 ± 0.01	5.18 ± 0.81	1.54 ± 0.08	1.43
[S24A] I11L	5	0.31 ± 0.00	4.58 ± 0.07	0.80 ± 0.03	0.74
[K25A] I11L	5	0.27 ± 0.00	4.80 ± 0.34	1.24 ± 0.06	1.15
[V26A] I11L	5	0.25 ± 0.01	14.75 ± 0.79	4.76 ± 0.70	4.41
[Y28A] I11L	6	0.29 ± 0.01	6.89 ± 0.36	1.83 ± 0.11	1.69
[K29A] I11L	6	0.27 ± 0.00	5.29 ± 0.32	1.02 ± 0.03	0.94
[N30A] I11L	6	0.27 ± 0.00	4.85 ± 0.27	0.67 ± 0.03	0.62
kB1	–	0.22 ± 0.00	18.2 ± 0.53	6.42 ± 0.59	–

[a] All data were done in triplicate and are mean ± SEM.
[b] Fold of activity loss in cytotoxicity for Ala mutants compared to I11L.

mutants, that is [V9A], [Y10A], and [L11A], which had five-to eight-fold less cytotoxic activity compared to I11L. Loop 3 mutants [F14A] and [I18A]I11L, loop 1 mutant [S7A], as well as the loop 5 mutant [V26A]I11L had approximately four-fold decreases in activity. Loop 6 mutants, [F2A] and [Y28A]I11L, only decreased activity by 1.5- to three-fold compared to I11L. Finally, loop 4 and 5 mutants as well as the loop 1 mutant [G5A]I11L were essentially as cytotoxic as the parent peptide. It is worth noting that [G1A], [S24A], and [N30A]I11L increased the cytotoxic potency by almost two-fold compared to I11L. In summary, the ranking of importance for cytotoxicity is, therefore, loop 2 > loop 3 > loop 1 ≥ loop 5 > loop 6 ≥ loop 4, paralleling the membrane activity results.

Discussion

This study was based on the discovery that mutation of Ile-11 to Leu substantially improves the *in vitro* folding yield of bracelet cyclotide hyen D without affecting bioactivity (24). To better understand the mode of action of I11L and the bracelet subfamily from which it originates, all Ala-mutants of I11L were synthesized and folded, and the effects of these single substitutions on folding and structure, membrane-binding activity, and cytotoxicity relative to I11L were evaluated. This first alanine scan mutagenesis study on a bracelet cyclotide provides insights into the SAR for the largest cyclotide subfamily.

The substitution of Ile for a Leu residue in loop 2 is a relatively conservative change and, therefore, it is surprising that it can improve *in vitro* folding yields. A potential explanation is that the native loop 2 sequence, which comprises either bulky (*i.e.*, Val, Ile, and Tyr) or rigid (*i.e.*, Pro) residues packed closely together, has poor conformational freedom, hindering sampling of the native structure during oxidative folding. It appears that a methyl on the Cγ (Leu) instead of Cβ (Ile) position is sufficient to relieve this structural frustration, decreasing the rigidity of loop 2 and increasing folding efficiency under standard cyclotide folding conditions. On top of its facile synthesis, the I11L mutant could adopt the same secondary structure as the WT hyen D, confirmed using NMR spectroscopy, and, therefore, I11L can serve as a template to examine the effects of alanine substitutions.

The alanine mutagenesis scan identified three additional residues that are critical to achieving the native fold under oxidative folding conditions and stabilizing the native structure. Of the alanine mutants that could be assembled, all adopted the native-like fold, except [E6A], [T15A], and [G19A]I11L. The importance of the Glu residue in folding is consistent with earlier studies on the folding of Möbius cyclotides. For example, synthetic variants of kB1 in which the Glu residue was substituted to Ala, Lys, and Asp residues had low yields (18, 21, 34). Analysis of the solution structure of hyen D showed that the Glu-6 sidechain (loop 1) forms a hydrogen bond with the hydroxyl group of Thr-15 sidechain (loop 3), which has also been observed in other bracelet cyclotide structures (13, 25, 26). The conservation of this interaction and its role in stabilizing the structure might partially explain why Thr-15 is as important as Glu-6 for enabling formation of the native structure. Gly-19 is the last residue of loop 3 and is highly conserved, with ∼90% of bracelet and Möbius cyclotides having a Gly residue in the same position. This conserved Gly has been observed to adopt a positive Φ-angle, which is thought to help minimize strain of the cyclic cystine knot structure (25, 35). The unsuccessful folding of [G19A]I11L in this study confirmed the importance of this Gly in the bracelet cyclotide structure. Aside from these three residues, we note that alanine substitution of polar residues, including [G1A], [G5A], [S7A], [S21A], [K23A], [K25A], and [K29A]I11L, remarkably reduced folding yields compared to I11L, suggesting that the overall sequence hydrophobicity also affects *in vitro* folding.

We identified several residues that are essential for the activity of I11L by evaluating the effect of substitutions on membrane binding and cancer cell cytotoxicity. Three of these residues are in loop 2 (Val-9, Tyr-10, Ile-11), two in loop 3 (Phe-14, Ile-18), one in loop 1 (Ser-7), and one in loop 5 (Val-26). The importance of loop 2 residues is consistent with a study from Burman *et al.* (32), in which a loop 2 Trp-hydroxylated cyO2 lost activity. Our findings suggest that Ser-7 in loop 1 and Val-26 in loop 5 are also critical for activity, a result that has not yet been reported for bracelet cyclotides. Surprisingly, despite being reported to be one of the functionally essential residues in kalata B1 (18, 21), Ala substitution of the Gly residue in loop 1 did not affect activity, suggesting that residues involved in the bioactive patch of bracelet cyclotides are different to those of Möbius cyclotides. We also discovered that a single mutation of the basic residues in loop 5 (Lys-23 and Lys-25) or loop 6 (Lys-29) did not affect the activity, corroborating the results from a study showing that masking of one basic residue, Arg on cyO2 using 1, 2-cyclohexanedione, did not affect bioactivity (36). However, it was reported that acetylation of two lysines or covering all three basic residues of cyO2 could cause decreases in activity by three to 18-fold (5, 36).

Overall, we identified that the residues in loops 1, 2, and 3 are critical for the folding and activity of I11L and wondered whether this finding is applicable to other bracelet cyclotides. According to CyBase (14), 252 bracelet cyclotides have been discovered at the protein level to date. As most of these bracelet cyclotides have the same number of residues in loops 1 and 2, but different numbers of residues in loop 3, we subgrouped the bracelet cyclotides according to their loop 3 length (see Fig. S5). We found that 166 bracelet cyclotides contain six residues in loop 3, 41 contain seven residues, 37 contain four residues, seven contain five residues, and one contains three residues. Based on this classification, I11L, hyen D, and cyO2 all belong to the largest subgroup of the bracelet cyclotide subfamily and cyO1 belongs to the second largest subgroup. Therefore, our study is relevant to the majority of bracelet cyclotides and provides new insights, as well as complementary information, to earlier studies on cyO2.

As both cyO1 and cyO2 have a 3_{10} helix in loop 3, which is a typical feature of bracelet cyclotides that distinguishes them

from Möbius cyclotides, we consider bracelet cyclotides with six or seven residues in loop 3 as typical bracelet cyclotides (207 out of 252 peptides in total). We analyzed the sequences of these cyclotides to identify whether our results are consistent with evolutionary trends. Figure 4 shows the sequence conservation of loops 1, 2, and 3 using a logo representation, and a sequence diversity wheel analysis is provided in Fig. S5. Our results show that Glu in loop 1, Thr (or Ser, both of them have a hydroxyl in sidechain) and Gly in loop three are essential for folding/structure, which is consistent with these residues being highly conserved as shown in Figure 4 (Thr is highlighted in orange; it is at the second position in the six-residue subgroup but at the third position in the seven-residue subgroup) (25). Our results also indicate that loops 2 and 3 are important for activity, with loop 2 being more important than loop 3, which is consistent with loop 2 being more conserved than loop 3 (Fig. 4). It has been noticed that loop 2 is always composed entirely of hydrophobic residues, possibly reflecting its role in mediating interaction with the hydrophobic membrane core for all the analyzed bracelets.

Based on these results, we propose a membrane-binding model of hyen D, which we speculate to be representative of the majority of bracelet cyclotides. Our model is also based on the proposed membrane-binding mode of kB1 (21) and an NMR study examining cyO2 binding to dodecylphosphocholine micelles (37). We define two faces on hyen D — one is the 'hydrophobic face' and the other is the 'bioactive face'. The hydrophobic face contains all loop 2 residues and three hydrophobic residues in loop 3 (patch highlighted in green, Fig. 5*A*). Figure 5*A* illustrates how parts of the hydrophobic face might be inserted into the membrane, specifically through residues Val-9, Tyr-10, Ile-11, Pro-12, and Phe-14 (dark green) as these residues cause a large decrease in potency when mutated. The other residues of the hydrophobic face, Ala-17 and Ile-18 (light green), possibly also assist in the membrane insertion. In this model, Val-26 of loop 5 and Phe-2 of loop 6 are not in proximity to the hydrophobic core of the membrane, even though the V26A and F2A substitutions resulted in a decrease in activity. However, as membrane binding is a dynamic process (38), it is possible that Val-26 and Phe-2 later come into contact with the membrane. In addition, these two residues are hydrophobic, and, therefore, substitution of either residue to Ala reduced the overall hydrophobicity, resulting in a loss of activity. There are three hydrophilic residues that were shown to be essential for the bioactivity and folding, including Glu-6, Ser-7, and Thr-15. These three residues are located in the bioactive face and are primed to contact lipid headgroups.

Similar to the Möbius cyclotide kB1, we propose that bracelet cyclotides display a hydrophobic face and a bioactive face, albeit the positions involved in these regions differ. First, the hydrophobic face comprises different residues, that is, loops 2, 5, and 6 for Möbius (Fig. 5*B* purple) and loops 2 and 3 for typical bracelet cyclotides. Second, the importance of these two faces is different. For Möbius cyclotides, the bioactive face was shown to be more important than the hydrophobic face because Ala substitution on bioactive face residues resulted in a total loss in insecticidal activity but mutations on the hydrophobic face did not (18). By contrast, we show that the hydrophobic face is more important than the bioactive face in bracelet cyclotides, suggesting differences in the binding mode of the two main subfamilies of cyclotides.

In summary, we report an alanine mutagenesis study of a bracelet cyclotide, identifying residues important for its structure and activity. Membrane-binding measurements and cytotoxicity assays pinpointed loops 2 and 3 to be the most critical for its function. Bringing these results together with other cyclotide studies, we propose that the mode of action for bracelet cyclotides involves a hydrophobic face and a bioactive face similar to that of Möbius cyclotides but distinctly different in some details because those faces involve different loops and residues. We therefore hypothesize the following mode of action for bracelet cyclotides: the bioactive face facilitates initial membrane binding and peptide localization on the membrane surface, and the subsequent interactions between the hydrophobic residues and the membrane core drives cyclotide insertion into the membrane. The insertion of cyclotides induces local disturbances in the lipid bilayer, causing membrane disintegration and thus leading to cell death. The study contributes valuable insights for future peptide-engineering studies using bracelet cyclotides.

Experimental procedures

Natural cyclotides extraction and isolation

H. enneaspermus for hyen D and *Oldenlandia affinis* for kB1 were ground into a fine powder and extracted with 50% acetonitrile (1% formic acid) overnight. The extracts were fractionated using Strata C18-E solid phase extraction

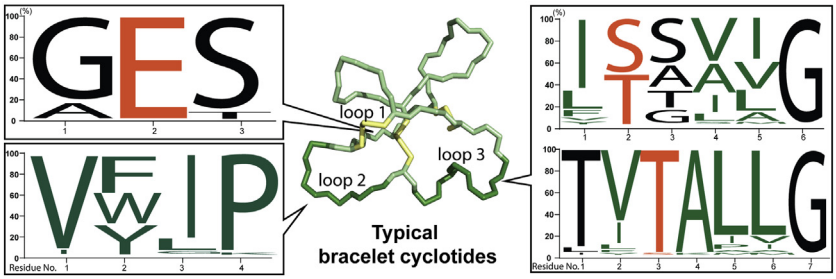

Figure 4. Sequence logo of functionally critical residues within typical bracelet cyclotides. For better alignment, the sequence logo of loop 3 was separated into six- and seven-residue subgroups. The conserved structurally critical residues are highlighted in *orange*, while hydrophobic residues are highlighted in *dark green*.

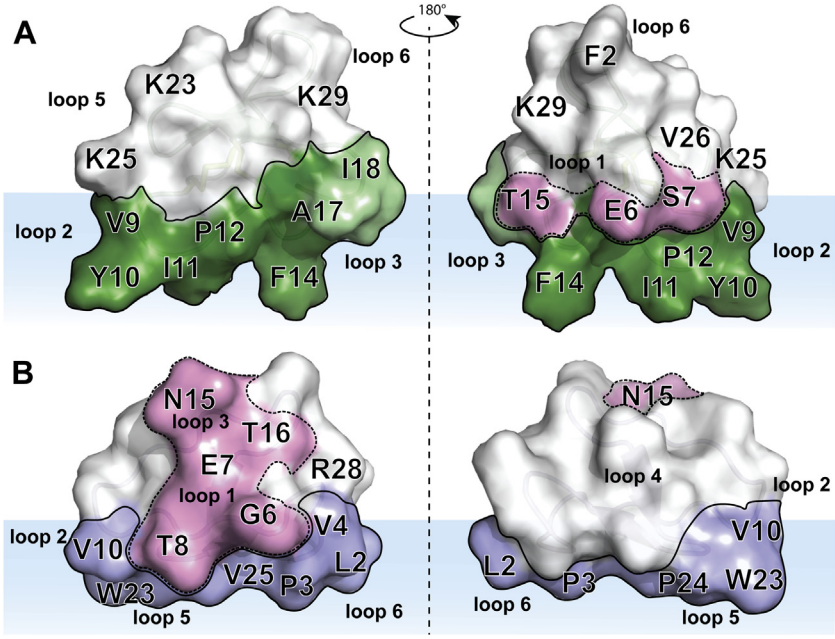

Figure 5. Schematic representation of the membrane-binding orientation of hyen D and kB1. The hydrophobic face and bioactive face are surrounded by *solid* and *dashed lines*, respectively. The bioactive faces of both molecules are highlighted in *pink*. *A*, the hydrophobic face for hyen D is shown in *green*. Residues in *light green* assist in membrane interaction, while residues in *dark green* are deeply inserted into the membrane. *B*, the hydrophobic face for kB1 is shown in *purple*. The *faint blue* area represents the potential location of the cell membrane depicting the interaction of the hydrophobic face of hyen D (or kB1) with the membrane.

cartridges. The cyclotides were concentrated in the 30 to 50% acetonitrile elution. Hyen D and kB1 were isolated by repetitive RP-HPLC, and their purity was above 95% as confirmed by analytical HPLC.

NMR solution structure of hyen D and NMR structure study of I11L and its variants

Each peptide was dissolved in 500 µl of H_2O and 50 µl of D_2O, with 1 µl (10 mg/ml) of 4, 4-dimethyl-4-silapentane-1-sulfonic acid as a reference. One-dimensional ^{1}H spectra and two-dimensional TOCSY and NOESY spectra were acquired for I11L and its variants using a Bruker ARX 600 NMR spectrometer (Bruker) at 298 K. For hyen D, 1D, TOCSY, NOESY, E-COSY, ^{13}C-HSQC, ^{15}N-HSQC, and TOCSY D_2O exchange experiments were acquired. The temperature coefficient data was adapted from a previous study (7). All NMR spectra were assigned using the CCPNMR program (version 2.4.2). Secondary Hα chemical shifts were calculated by subtracting random coil chemical shift values from the measured Hα chemical shifts for all residues (28). The sample pH for secondary Hα chemical shift determination was in the range 3 to 3.5.

For hyen D 3D structure calculations, distance restraints were derived from cross-peaks in NOESY spectra. Backbone dihedral angle restraints were derived from $^{3}J_{HNH\alpha}$ coupling constant values measured from peak splitting in the 1D spectrum. Side chain χ^{1} dihedral angles were derived from $^{3}J_{H\alpha H\beta}$ from the E-COSY spectrum together with NOE intensities. After initial structure calculations were performed with CYANA (39), hydrogen-bond restraints for slowly exchanging amides derived from D_2O exchange and temperature coefficient were added. The final set of 50 structures was calculated using a torsion angle-simulated annealing protocol within CNS (40), during which the structures of hyen D were refined in a water shell. The structures were analyzed with MOLMOL (41) and PROCHECK (42), and the 20 lowest-energy structures were deposited in the Protein Data Bank (PDB ID: 7RN3).

Synthesis and folding of I11L and its alanine mutants

The designed I11L alanine variants were chemically assembled using Fmoc solid-phase synthesis as previously described (43). Briefly, the linear precursors were assembled on an automatic peptide synthesizer (Symphony, Protein Technologies) and then cleaved from 2-CTC resin using 1% TFA in dichloromethane. The sidechain-protected linear precursors were subsequently cyclized using 1-[Bis(dimethylamino)methylene]-1H-1,2,3-triazolo[4,5-b]pyridinium 3-oxid hexafluorophosphate and N,N-diisopropylethylamine in dimethylformamide at room temperature for 6 h. Side chain deprotection was carried out in triisopropylsilane: H_2O: TFA (2:2:96, v/v/v). The crude cyclic peptides were purified *via* RP-HPLC and folded in a standard cyclotide folding buffer containing 50% isopropanol, 0.1 M ammonium bicarbonate (pH 8.5), 2 mM reduced glutathione, and 0.8 mM oxidized glutathione; incubated at 25 °C for 12 h. I11L was folded in a slightly different condition as follows: 45.5% isopropanol, 0.1 M ammonium bicarbonate, pH 8.5, 2 mM reduced glutathione, 0.8 mM oxidized glutathione, incubated at 25 °C for 12 h. Correctly folded cyclotides were purified *via* RP-HPLC,

and their purity was checked on analytical HPLC. The yield of correctly folded peptides was calculated by comparing the area of the peptide peak to the total area from the analytical HPLC trace. The yield of correctly folded peptides was calculated by comparing the area of the peptide peak to the total area from the analytical HPLC trace. The folding yield of each alanine mutant was then compared to that of I11L (44%) and the relative percentage is shown in Table 2.

Evaluation of membrane binding activity of I11L variants

Synthetic lipids were obtained from Avanti Polar-Lipids. The assay was performed as previously described (7). Briefly, homogeneous small unilamellar vesicles of POPC/POPE (80:20) prepared in the SPR running buffer (10 mM Hepes, 150 mM NaCl, pH 7.4, filtered) were obtained by repetitively extruding through a 50 nm pore size polycarbonate membrane. To monitor peptide–lipid interactions in real time, BIAcore 3000 instrument was used. The peptides solution was injected and monitored for 10 min after the POPC/POPE lipid was loaded onto an L1 sensor chip and formed the lipid bilayer. Peptides were tested at concentrations ranging from 4 to 128 μM. The peptide-to-lipid molar ratio and K_D values were calculated with GraphPad Prism software (version 9.0.0) by fitting using the "specific binding with Hill slope" option.

Cytotoxicity evaluation of I11L variants

The cytotoxicity of the peptides was evaluated using the resazurin assay. Assays were performed as previously described (7). HeLa cells were seeded at 5000 cells/well into a 96-well flat-bottomed plate one day prior to adding the peptides. All the peptides were dissolved in water and tested at concentrations ranging from 16 to 0.0625 μM in triplicate. 1% Triton X and water were applied as positive and negative control, respectively. After 24 h incubation, resazurin (0.05%, w/v) was added and incubated with cells for another 18 h. Absorbance was measured at 540 and 620 nm (Tecan M1000 Pro plate reader, Labsystems). The percentage of cell death was quantified by calculating the absorbance ratio, R (R= absorbance at 620/540), and applying the following equation: % Cell death = $(R_{sample} - R_{H2O})/(R_{TX} - R_{H2O}) \times 100$. Data were analyzed with GraphPad Prism software (version 8.3.1) using "Specific binding with Hill slope" algorithm.

Data availability

The hyen D three-dimensional structure is deposited in the PDB: PDB identifier 7RN3.

Supporting information—This article contains supporting information.

Acknowledgments—The work was supported by access to facilities by the Australian Government through the National Collaborative Research Infrastructure Strategy (NCRIS) and the Australian Research Council Centre of Excellence for Innovations in Peptide and Protein Science (CE200100012). We thank Edward Gilding for collecting *H. enneaspermus*; Lai Yue Chan, Johannes Koehbach, and Simon de Veer for their assistance in peptide synthesis; and Robyn Craik for article proofreading.

Author contributions—Q. D., Y.-H. H., and D. J. C. conceptualization; Q. D., Y.-H. H., and D. J. C. methodology; Q. D., Y.-H. H., and C. K. W. investigation; Q. D., Y.-H. H., and C. K. W. formal analysis; Q. D., Y.-H. H., and C. K. W. data curation; Q. D. writing–original draft; Y.-H. H., C. K. W., Q. K., and D. J. C. writing–review and editing; D. J. C. funding acquisition; Y.-H. H. and D. J. C. project administration.

Funding and additional information—D. J. C. is supported by an Australian Research Council (ARC) Australian Laureate Fellowship (FL150100146). Q. D. is supported by the Chinese Scholarship Council.

Conflict of interest—The authors declare that they have no conflicts of interest with the contents of this article.

Abbreviations—The abbreviations used are: cyO2, cycloviolacin O2; E-COSY, exclusive COSY; HSQC, heteronuclear single quantum coherence; POPC, 1-palmitoyloleoyl-phosphatidylcholine; POPE, 1-palmitoyloleoyl-phosphatidylethanolamine; SAR, structure-activity relationship; SPR, surface plasmon resonance.

References

1. de Veer, S. J., Kan, M.-W., and Craik, D. J. (2019) Cyclotides: From structure to function. *Chem. Rev.* **119**, 12375–12421
2. Huang, Y.-H., Du, Q., and Craik, D. J. (2019) Cyclotides: Disulfide-rich peptide toxins in plants. *Toxicon* **172**, 33–44
3. Craik, D. J., Daly, N. L., Bond, T., and Waine, C. (1999) Plant cyclotides: A unique family of cyclic and knotted proteins that defines the cyclic cystine knot structural motif. *J. Mol. Biol.* **294**, 1327–1336
4. Slazak, B., Kapusta, M., Strömstedt, A. A., Słomka, A., Krychowiak, M., Shariatgorji, M., Andrén, P. E., Bohdanowicz, J., Kuta, E., and Göransson, U. (2018) How does the sweet violet (Viola odorata L.) fight pathogens and pests - cyclotides as a comprehensive plant host defense system. *Front. Plant Sci.* **9**, 1296
5. Colgrave, M. L., Kotze, A. C., Ireland, D. C., Wang, C. K., and Craik, D. J. (2008) The anthelmintic activity of the cyclotides: Natural variants with enhanced activity. *Chembiochem* **9**, 1939–1945
6. Wang, C. K., Colgrave, M. L., Gustafson, K. R., Ireland, D. C., Göransson, U., and Craik, D. J. (2008) Anti-HIV cyclotides from the chinese medicinal herb Viola yedoensis. *J. Nat. Prod.* **71**, 47–52
7. Du, Q., Chan, L. Y., Gilding, E. K., Henriques, S. T., Condon, N. D., Ravipati, A. S., Kaas, Q., Huang, Y.-H., and Craik, D. J. (2020) Discovery and mechanistic studies of cytotoxic cyclotides from the medicinal herb Hybanthus enneaspermus. *J. Biol. Chem.* **295**, 10911–10925
8. Gründemann, C., Koehbach, J., Huber, R., and Gruber, C. W. (2012) Do plant cyclotides have potential as immunosuppressant peptides? *J. Nat. Prod.* **75**, 167–174
9. Du, Q., Huang, Y.-H., Bajpai, A., Frosig- Jorgensen, M., Zhao, G., and Craik, D. J. (2020) Evaluation of the *in vivo* aphrodisiac activity of a cyclotide extract from Hybanthus enneaspermus. *J. Nat. Prod.* **83**, 3736–3743
10. Hernandez, J.-F., Gagnon, J., Chiche, L., Nguyen, T. M., Andrieu, J.-P., Heitz, A., Trinh Hong, T., Pham, T. T. C., and Le Nguyen, D. (2000) Squash trypsin inhibitors from momordica cochinchinensis exhibit an atypical macrocyclic structure. *Biochemistry* **39**, 5722–5730
11. Jennings, C. V., Rosengren, K. J., Daly, N. L., Plan, M., Stevens, J., Scanlon, M. J., Waine, C., Norman, D. G., Anderson, M. A., and Craik, D. J.

(2005) Isolation, solution structure, and insecticidal activity of kalata B2, a circular protein with a twist: Do Möbius strips exist in nature? *Biochemistry* **44**, 851–860
12. Saether, O., Craik, D. J., Campbell, I. D., Sletten, K., Juul, J., and Norman, D. G. (1995) Elucidation of the primary and three-dimensional structure of the uterotonic polypeptide kalata B1. *Biochemistry* **34**, 4147–4158
13. Göransson, U., Herrmann, A., Burman, R., Haugaard-Jönsson, L. M., and Rosengren, K. J. (2009) The conserved Glu in the cyclotide cycloviolacin O2 has a key structural role. *Chembiochem* **10**, 2354–2360
14. Wang, C. K., Kaas, Q., Chiche, L., and Craik, D. J. (2007) CyBase: A database of cyclic protein sequences and structures, with applications in protein discovery and engineering. *Nucleic Acids Res.* **36**, D206–D210
15. Kaas, Q., and Craik, D. J. (2010) Analysis and classification of circular proteins in CyBase. *Pept. Sci.* **94**, 584–591
16. Lindholm, P., Göransson, U., Johansson, S., Claeson, P., Gullbo, J., Larsson, R., Bohlin, L., and Backlund, A. (2002) Cyclotides: A novel type of cytotoxic agents. *Mol. Cancer Ther.* **1**, 365–369
17. Tang, J., Wang, C. K., Pan, X., Yan, H., Zeng, G., Xu, W., He, W., Daly, N. L., Craik, D. J., and Tan, N. (2010) Isolation and characterization of cytotoxic cyclotides from Viola tricolor. *Peptides* **31**, 1434–1440
18. Simonsen, S. M., Sando, L., Rosengren, K. J., Wang, C. K., Colgrave, M. L., Daly, N. L., and Craik, D. J. (2008) Alanine scanning mutagenesis of the prototypic cyclotide reveals a cluster of residues essential for bioactivity. *J. Biol. Chem.* **283**, 9805–9813
19. Svangård, E., Burman, R., Gunasekera, S., Lövborg, H., Gullbo, J., and Göransson, U. (2007) Mechanism of action of cytotoxic cyclotides: Cycloviolacin O2 disrupts lipid membranes. *J. Nat. Prod.* **70**, 643–647
20. Gerlach, S. L., Chandra, P. K., Roy, U., Gunasekera, S., Göransson, U., Wimley, W. C., Braun, S. E., and Mondal, D. (2019) The membrane-active phytopeptide cycloviolacin O2 simultaneously targets HIV-1-infected cells and infectious viral particles to potentiate the efficacy of antiretroviral drugs. *Medicines* **6**, 33
21. Huang, Y.-H., Colgrave, M. L., Clark, R. J., Kotze, A. C., and Craik, D. J. (2010) Lysine-scanning mutagenesis reveals an amendable face of the cyclotide kalata B1 for the optimization of nematocidal activity. *J. Biol. Chem.* **285**, 10797–10805
22. Shenkarev, Z. O., Nadezhdin, K. D., Sobol, V. A., Sobol, A. G., Skjeldal, L., and Arseniev, A. S. (2006) Conformation and mode of membrane interaction in cyclotides. *FEBS J.* **273**, 2658–2672
23. Henriques, S. T., Huang, Y.-H., Chaousis, S., Sani, M.-A., Poth, Aaron G., Separovic, F., and Craik, David J. (2015) The prototypic cyclotide kalata B1 has a unique mechanism of entering cells. *Chem. Biol.* **22**, 1087–1097
24. Huang, Y.-H., Du, Q., Jiang, Z., King, G. J., Collins, B. M., Wang, C. K., and Craik, D. J. (2021) Enabling efficient folding and high-resolution crystallographic analysis of bracelet cyclotides. *Molecules* **26**, 5554
25. Rosengren, K. J., Daly, N. L., Plan, M. R., Waine, C., and Craik, D. J. (2003) Twists, knots, and rings in proteins structural definition of the cyclotide framework. *J. Biol. Chem.* **278**, 8606–8616
26. Plan, M. R., Rosengren, K. J., Sando, L., Daly, N. L., and Craik, D. J. (2010) Structural and biochemical characteristics of the cyclotide kalata B5 from Oldenlandia affinis. *Pept. Sci.* **94**, 647–658
27. Daly, N. L., Clark, R. J., Göransson, U., and Craik, D. J. (2003) Diversity in the disulfide folding pathways of cystine knot peptides. *Lett. Pept. Sci.* **10**, 523–531
28. Wishart, D. S., Bigam, C. G., Holm, A., Hodges, R. S., and Sykes, B. D. (1995) 1 H, 13 C and 15 N random coil NMR chemical shifts of the common amino acids. I. Investigations of nearest-neighbor effects. *J. Biomol. NMR* **5**, 67–81
29. Wishart, D. S., Sykes, B. D., and Richards, F. M. (1992) The chemical shift index: A fast and simple method for the assignment of protein secondary structure through NMR spectroscopy. *Biochemistry* **31**, 1647–1651
30. Henriques, S. T., Huang, Y.-H., Castanho, M. A., Bagatolli, L. A., Sonza, S., Tachedjian, G., Daly, N. L., and Craik, D. J. (2012) Phosphatidylethanolamine-binding is a conserved feature of cyclotide-membrane interactions. *J. Biol. Chem.* **287**, 33629–33643
31. Burman, R., Strömstedt, A. A., Malmsten, M., and Göransson, U. (2011) Cyclotide–membrane interactions: Defining factors of membrane binding, depletion and disruption. *Biochim. Biophys. Acta* **1808**, 2665–2673
32. Burman, R., Herrmann, A., Tran, R., Kivelä, J.-E., Lomize, A., Gullbo, J., and Göransson, U. (2011) Cytotoxic potency of small macrocyclic knot proteins: Structure–activity and mechanistic studies of native and chemically modified cyclotides. *Org. Biomol. Chem.* **9**, 4306–4314
33. Tan, L. T.-H., Chan, K.-G., Pusparajah, P., Lee, W.-L., Chuah, L.-H., Khan, T. M., Lee, L.-H., and Goh, B.-H. (2017) Targeting membrane lipid a potential cancer cure? *Front. Pharmacol.* **8**, 1–12
34. Wang, C. K., Clark, R. J., Harvey, P. J., Johan Rosengren, K., Cemazar, M., and Craik, D. J. (2011) The role of conserved Glu residue on cyclotide stability and activity: A structural and functional study of kalata B12, a naturally occurring Glu to Asp mutant. *Biochemistry* **50**, 4077–4086
35. Wang, C. K., Hu, S. H., Martin, J. L., Sjögren, T., Hajdu, J., Bohlin, L., Claeson, P., Göransson, U., Rosengren, K. J., Tang, J., Tan, N. H., and Craik, D. J. (2009) Combined X-ray and NMR analysis of the stability of the cyclotide cystine knot fold that underpins its insecticidal activity and potential use as a drug scaffold. *J. Biol. Chem.* **284**, 10672–10683
36. Herrmann, A., Svangård, E., Claeson, P., Gullbo, J., Bohlin, L., and Göransson, U. (2006) Key role of glutamic acid for the cytotoxic activity of the cyclotide cycloviolacin O2. *Cell Mol. Life Sci.* **63**, 235–245
37. Wang, C. K., Colgrave, M. L., Ireland, D. C., Kaas, Q., and Craik, D. J. (2009) Despite a conserved cystine knot motif, different cyclotides have different membrane binding modes. *Biophys. J.* **97**, 1471–1481
38. Lei, X., Liu, S., Zhou, R., and Meng, X.-Y. (2021) Molecular dynamics simulation study on interactions of cycloviolacin with different phospholipids. *J. Phys. Chem. B.* **125**, 3476–3485
39. Güntert, P., Mumenthaler, C., and Wüthrich, K. (1997) Torsion angle dynamics for NMR structure calculation with the new program DYANA. *J. Mol. Biol.* **273**, 283–298
40. Brunger, A. T. (2007) Version 1.2 of the crystallography and NMR system. *Nat. Protoc.* **2**, 2728–2733
41. Koradi, R., Billeter, M., and Wüthrich, K. (1996) Molmol: A program for display and analysis of macromolecular structures. *J. Mol. Graph.* **14**, 51–55
42. Williams, C. J., Headd, J. J., Moriarty, N. W., Prisant, M. G., Videau, L. L., Deis, L. N., Verma, V., Keedy, D. A., Hintze, B. J., and Chen, V. B. (2018) MolProbity: More and better reference data for improved all-atom structure validation. *Protein Sci.* **27**, 293–315
43. Cheneval, O., Schroeder, C. I., Durek, T., Walsh, P., Huang, Y.-H., Liras, S., Price, D. A., and Craik, D. J. (2014) Fmoc-based synthesis of disulfide-rich cyclic peptides. *J. Org. Chem.* **79**, 5538–5544